Pergamon

Int. J. Heat Mass Transfer. Vol. 40, No. 15, pp. 3513–3525, 1997

Printed in Great Britain
0017–9310/97 $17.00+0.00

PII: S0017–9310(97)00023–9

Time-varying heat transfer coefficients between tube-shaped casting and metal mold

TAE-GYU KIM and ZIN-HYOUNG LEE†

Department of Materials Science and Engineering, RASOM, Korea Advanced Institute of Science and Technology, 373-1 Kusong-dong, Yusong-ku, Taejon, 305-701, Korea

(*Received* 29 *January* 1996 *and in revised form* 6 *January* 1997)

Abstract—An experimental and numerical study were made on the time-varying heat transfer coefficient $h(t)$ between a tube-shaped casting and metal molds. One dimensional treatment was adopted in analyzing the heat flows between the casting and the inner and the outer mold. The sequential function specification method was employed to solve the nonlinear inverse heat conduction problem. In order to investigate the different behavior of $h(t)$ for different alloys, casting experiments were carried out with three Al-base alloys and pure Al having different types of solidification behavior. It was found that the temperature change of the outer mold showed a normal heating and cooling curve. However, that of the inner mold was unusual especially for the alloys with a wide solidification range, i.e. the temperature increases first rapidly, then halts for a while and then increases again showing finally a regular heating and cooing curve. The resulting heat transfer coefficient at the interface to the inner mold $h_i(t)$ decreases temporarily and then increases, while the one at the interface to the outer mold $h_o(t)$ decreases monotonously to a quasi steady state. The abnormal heat transfer phenomenon at the inner interface for the alloys with a wide solidification range was concluded to be caused by a slight movement of the semi-solid inner wall at the inside of the tube-shaped casting due to the solidification contraction of the casting freezing in a mushy type.

1. INTRODUCTION

During the solidification of metal casting, heat transfer resistance at the interface between the casting and the mold depends on many factors, such as contacting pressure [1], oxides on surfaces, roughness of surfaces, coating material, coating thickness and gap formation due to the deformation of casting and mold [2], to name a few. The effect of the heat transfer coefficient (inverse value of the thermal resistance) at the mold/casting interface and its time dependence on the solidification are of prime importance, especially for castings in metal molds. The solidification process of the castings in the metal molds can be simulated by computer if the heat transfer coefficients $h(t)$ at the casting/mold interfaces are made available. To determine the heat transfer coefficient, it is necessary to develop a mathematical method which enables a calculation of the coefficient at the interface from measurable quantities, such as thermal histories at various thermocouple locations.

If the heat flux or the temperature history at the surface of a solid are unknown, they should be estimated inversely by solving the heat conduction problem (inverse heat conduction problem, IHCP) from the measured temperature histories inside of a body.

One of the earliest papers on the IHCP by Stolz [3] addressed the calculation of heat transfer rates during quenching of bodies with simple finite shapes. Frank [4] suggested a least-square method for determining the rate of surface heat input which best fits the interior experimental temperature data. Beck [5] developed the basic concepts that permitted much smaller time steps than the Stolz method and stabilized the inverse problem by using future temperatures (measured temperature after the instant when the heat flux is to be determined) in a least-square minimization procedure. Ho and Pehlke [6] studied interfacial heat transfer on two types of castings with different locations of copper chill. In order to calculate the interfacial heat transfer coefficient, they adopted an implicit finite difference formulation with the enthalpy method, based on the nonlinear estimation technique. Nishida *et al.* [2] calculated the heat transfer coefficient for the outer surface of a cylindrical casting of Al and Al-alloys.

There are many articles concerning the heat transfer coefficient at the interface between castings and outer molds. However, the studies on the effect of a core or an inner mold are scarce. The purpose of this study is to determine simultaneously the interfacial heat transfer coefficients at the inside and the outside interface of a tube-shaped casting. Toward this end, laboratory casting experiments have been made together with the computational study. For the calculation of transient interfacial heat transfer coefficients at the interface between the casting and each of the inner and the outer mold, the sequential function specification procedure proposed by Beck was adopted [7]. The characteristics

† Author to whom correspondence should be addressed.

NOMENCLATURE

d	thickness of coating or air gap
$h(t)$, $h_i(t)$, $h_o(t)$	unknown heat transfer coefficient at the casting-mold interface
$h_{im}(T)$	heat transfer coefficient from the inner mold to the air
$h_{om}(T)$	heat transfer coefficient from the outer mold to the air
H	total enthalpy of the casting
k	thermal conductivity of the casting
$k_m(T)$	thermal conductivity of the mold
p	number of future times
r	radial coordinate
R_i, R_o	inner radius of the inner mold and outer radius of the outer mold
S	the sum of the least square error
t	time
T	calculated temperature
T_{air}	temperature of environment
T_{ca}	interface temperature of the casting
T_{im}, T_{om}	interface temperature of the inner mold and the outer mold
Y	measured temperature.

Greek symbol

ρ	density.

Subscripts

c	coating
g	gap
i	inside interface
$M+i$	time index ($i = 1, \ldots, p$)
o	outside interface.

of the time-varying heat transfer coefficients at the interfaces were discussed in the view of thermal deformation, solidification contraction, solidification range and solidification types.

2. CASTING EXPERIMENTS

A set of molds for a tube-shaped casting, as shown in Fig. 1, was made of hot worked die steel (SKD61). Sheathed thermocouples of K-type with 1.5 mm diameter were inserted into the holes with 1.6 mm diameter and 30 mm depth for the measurement of mold temperature. The thermocouples were pushed slightly against the bottom of the holes in the molds with a spring to attain a good contact to the mold. The tolerance of the positions of the holes were ± 0.1 mm. The thermocouples, numbers 3 and 4 (TC3 and 4 as shown in Fig. 1) in the casting were positioned accurately in the die cavity with a thermocouple holder prior to pouring. Top surfaces of the molds

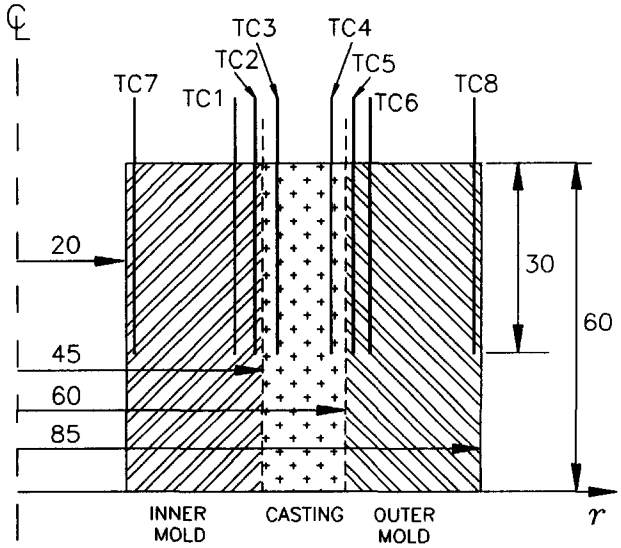

TC#	DISTANCE from CENTER	TC#	DISTANCE from CENTER
TC7	22 mm	TC4	56 mm
TC1	40 mm	TC5	62 mm
TC2	43 mm	TC6	65 mm
TC3	49 mm	TC8	83 mm

Fig. 1. Experimental setup for a tube-shaped casting.

Table 1. Chemical composition and solidification type of cast metals

Material	Si	Cu	Mg	Fe	Ni	Al	Soldification type [8]
AC8A	12.7	1.2	1.2	—	1.1	Bal.	Mushy
A356	7	0.2	0.3	0.2	0.05	Bal.	Primary : mushy Eutectic : shell forming
Pure Al	—	—	—	—	—	99.7	Shell forming
Al–Si eutectic	12.6	—	—	—	—	Bal.	Shell forming

Table 2. Thermophysical properties of casting alloys and mold [9]

Material	AC8A	A356	Pure Al	Al–Si eutectic	SKD61 steel
Density at 20°C (kg m^{-3})	2173	2685	2700	2710	7850
Specific heat at 100°C (J kg^{-1} K^{-1})	963	963	917	972	483
Thermal conductivity at 25°C (W m^{-1} K^{-1})	145	159	238	141	$k_m = 47–2.74 \ln (T°C)$
Latent heat of fusion at (kJ kg^{-1})	389	389	397	389	—
Liquidus temperature (°C)	565	615	660	577	—
Solidus temperature (°C)	540	555			

and the casting were insulated with ceramic paper, and the base was made of insulating brick to attain one-dimensional heat flow in the radial direction.

Table 1 shows the chemical composition and the solidification type of cast metals selected to study the effect of different solidification types on the heat transfer coefficients at the interfaces. The melt was prepared in an electric resistance furnace. The pouring temperature of AC8A, A356 and Al–Si eutectic alloy were about 770°C, and that of pure aluminum was about 820°C. The molten metal was poured into the mold in about 3 s. The temperature of the casting and the molds were measured and logged onto the hard disk of the computer, and then were used for calculating the interfacial heat transfer coefficients. A data acquisition system and eight sheathed thermocouples were used for measuring the temperature at 100 ms intervals.

The properties of the cast metals and the mold are listed in Table 2. The thermal conductivity of the mold was considered as a function of temperature [9]. In order to investigate the coating effect, AC8A alloy casting experiments were carried out with a graphite base coating (TOYOCA-ACE GR-851) and a white coating (FOSECO-DYCOTE 39). The graphite coating was sprayed using a spray gun, and the white coating was brushed evenly. The coating thickness was around 70 and 100 μm for the graphite and the white coating, respectively. The thermal properties of coatings depend on the materials (minerals, powder size, binder, dilution etc.) as well as the porosity and the thickness of the coating, and can be measured effectively with melt filled in the mold. The voids at the mold/coating interface and the porosity in the coating itself have a great effect on the thermal conductivity of the coating. The voids at the coating/melt interface have also a big effect, and depend on the gas evolution from the coating, surface tension of the melt at the melt/coating interface and the pressure in the melt. It is therefore difficult to predict the exact thermal properties of coatings. In the present study, the calculated interfacial heat transfer coefficients are the result of the total heat transfer resistance at the casting/mold interface including coating, oxide skin, voids and gap.

3. METHOD OF SOLUTION

The Fourier heat conduction equation was inversely solved subject to the initial and boundary conditions

$$\rho \frac{\partial H}{\partial t} = \frac{1}{r} \frac{\partial}{\partial r} \left(kr \frac{\partial T}{\partial r} \right) \tag{1}$$

where the total enthalpy H can be split into the sensible and latent heat components. Equation (1) was discretized by implicit finite difference formulation based on the enthalpy method [10]. The relation that holds at the inside and the outside interface is expressed as

$$-k_m(T) \left. \frac{\partial T(r,t)}{\partial r} \right|_{\mathrm{i}} = h_{\mathrm{i}}(t)[T_{\mathrm{im}} - T_{\mathrm{ca}}] \tag{2a}$$

$$-k_m(T) \left. \frac{\partial T(r,t)}{\partial r} \right|_{\mathrm{o}} = h_{\mathrm{o}}(t)[T_{\mathrm{ca}} - T_{\mathrm{om}}]. \tag{2b}$$

The boundary conditions on the cylindrical surfaces of the molds facing to air are

$$-k_m(T) \left. \frac{\partial T(r,t)}{\partial r} \right|_{r=R_{\mathrm{i}}} = h_{\mathrm{im}}(T)[T_{\mathrm{air}} - T(R_{\mathrm{i}}, t)] \tag{3a}$$

$$-k_m(T)\left.\frac{\partial T(r,t)}{\partial r}\right|_{r=R_o} = h_{om}(T)[T(R_o,t)-T_{air}] \tag{3b}$$

where $h_{im}(T)$ and $h_{om}(T)$ denote the inside and outside heat transfer coefficients to air, respectively. These are calculated from the surface temperature of each mold by including the convection and the radiation heat transfer to air:

$$h_{im}(T) = h_{air}+\varepsilon\sigma[T(R_i,t)+T_{air}][T(R_i,t)^2+T_{air}^2] \tag{4a}$$

$$h_{om}(T) = h_{air}+\varepsilon\sigma[T(R_o,t)+T_{air}][T(R_o,t)^2+T_{air}^2] \tag{4b}$$

where ε and σ denote emissivity (0.8) and Stefan–Boltzmann constant (5.67×10^{-8} W m^{-2} K^{-4}), and h_{air} and T_{air} are 15 W m^{-2} K^{-1} and 297 K, respectively. As the initial condition, an instantaneous filling of the mold was assumed and uniform initial temperatures in the casting (maximum temperature measured in the casting during pouring) and the molds (20°C) were assumed.

One way to solve the inverse heat conducting problem (IHCP) is to assume a functional form of the interfacial heat transfer coefficient variation with time. This is called the function specification method [7]. The function can be a sequence of constant segments or of other forms such as straight line segments, parabolas, etc. The sequential function specification procedure proposed by Beck is to assume temporarily that several future heat transfer coefficients are time-invariant [7, 11]. The procedure of Beck [7] depends on the minimization, at regular finite time step, of the following function:

$$S = \sum_{i=1}^{p}(Y_{M+i}-T_{M+i})^2 \tag{5}$$

where Y_{M+i} and T_{M+i} represent the measured and calculated temperatures at various times, respectively, and p denotes the number of future time. The use of future temperature improves greatly the stability of IHCP algorithm and reduces substantially the sensitivity to measurement errors [11]. The algorithm with one future temperature is used in the present analysis. Further discussion of this method is compiled by Beck *et al.* [7, 11]. The transient heat transfer coefficients were calculated for every 1 s interval from the time of pouring to 80 s after pouring. It was found that a greater number of future temperatures is necessary to improve the stability if a time increment smaller than 1 s is used. The increment of 1 s was selected to get more stable and faster results.

Among the heating curves obtained from the six thermocouples in the molds (Fig. 1), the ones measured nearest (2 mm apart) to the interface were used as the known temperature history for calculating the interfacial heat transfer coefficients; i.e the heating curve from the thermocouple TC2 was used to calculate $h_i(t)$, and the heating curve from the thermocouple TC5 was used in calculating $h_o(t)$. The measured temperature curves from the other thermocouples were used to test the accuracy of the calculated $h(t)$.

4. EXPERIMENTAL RESULTS

The results of five typical casting experiments are presented here. The casting experiments with AC8A alloy with the graphite coating and the white coating are examined first, followed by those with A356 alloy, pure Al, and Al–Si binary eutectic alloy in the mold with the graphite coating.

4.1. *AC8A alloy casting and the effect of coatings*

Figure 2(a) shows the changes of temperature in the casting and the mold with the graphite coating for AC8A alloy. The cooling curves of the casting (TC3 and 4) and the heating curves of the outer mold (TC5, 6 and 8) are as expected. However, the heating curves in the inner mold (TC1 and 2) show an abnormal behavior, i.e. the temperature increases first rapidly, then halts after about 8 s for about 12 s and then increases again to approach the casting temperature. The solidification time of the casting (at the thermal center) is about 23 and 32 s in the graphite and the white coating, respectively.

Next the experiment with AC8A alloy was performed with the white coating and the results are shown in Fig. 2(b). The curves are very similar to those for graphite coating, except that the solidification time increased. It may be attributed to the larger thermal resistance of the white coating than that of the graphite coating. To make clear the difference of heat transfer through the two coating materials, the calculated heat transfer coefficients at both interfaces are shown in Fig. 3. The maximum outside heat transfer coefficient $h_o(t)$ is about 2700 W m^{-2} K^{-1} or 1500 W m^{-2} K^{-1} with the graphite or the white coating. The $h_o(t)$ decreases rapidly when a self-sustaining outside wall has solidified in the casting and a gap between the casting and the mold will grow due to the thermal expansion of the mold and the thermal contraction of the casting. The $h_o(t)$ decreases down to about 250 W m^{-2} K^{-1} in 30 or 40 s and then stays almost constant because the gap would not grow any more, as the temperature of the outer mold decreases and the casting contraction is restricted due to the expanding inner mold. The fast decrease of $h_o(t)$ occurs later for the white coating, as the self-sustaining outside wall forms later because of the slower heat transfer across the white coating.

The general shape of $h_i(t)$ for the white coating is similar to the graphite coating, as shown in Fig. 3(b). The initial maximum $h_i(t)$ is close to that of $h_o(t)$. The temporary drop in $h_i(t)$ appears in both coatings as can be expected from the abnormal heating curves of Fig. 2. After this, $h_i(t)$ starts increasing again near the

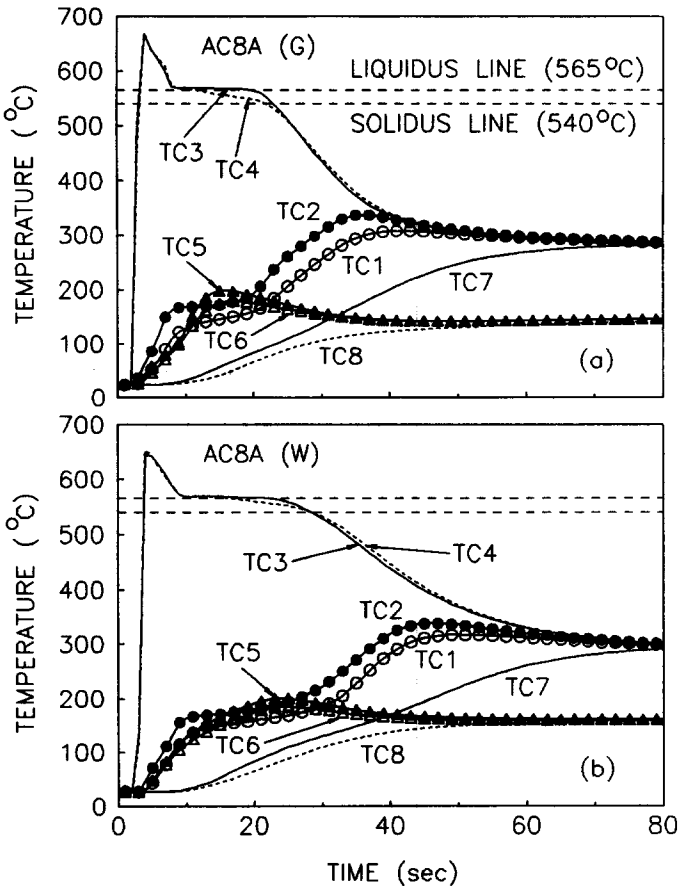

Fig. 2. Measured temperatures vs time for AC8A alloy casting: (a) with the graphite coating; (b) with the white coating (note that G means graphite coating and W means white coating).

end of the solidification of the casting and increases very high up to 20 000 or 40 000 W m^{-2} K^{-1} due to the contraction of the casting onto the expanding inner mold.

4.2. *A356 alloy casting*

The experimental result for A356 alloy casting in the graphite-coated mold is shown in Fig. 4(a). The abnormal behavior of the heating curves of the inner mold is also seen in this case, showing even a short period of temperature drop (TC2).

The shape of $h_o(t)$ curve in Fig. 4(b) is similar to AC8A (Fig. 3(a)), and the maximum $h_o(t)$ is nearly 2900 W m^{-2} K^{-1}. The $h_i(t)$ shows a temporal drop during the initial solidification also in this alloy as seen in the AC8A alloy case. The phenomenon seems to be related to the wide solidification range of these alloys and will be discussed later in detail.

4.3. *Pure Al and Al–Si binary eutectic with congruent melting temperature*

To investigate the effect of the solidification types on the unusual heat transfer behavior at the inner mold, casting experiments with pure Al and Al–12.6%Si binary eutectic alloy with congruent melting temperature were performed with the graphite coating. The temperature-time curves and $h(t)$ for pure Al and Al–Si binary eutectic alloy are shown in Figs. 5 and 6. Notice that the temperature of the inner mold (TC1 and 2) increases without any holding period and the $h_i(t)$ increases continuously, which is a normal case and can be easily explained with the thermal expansion of the mold and the thermal contraction of the solidified shell of the casting, and the contacting pressure between the casting and the inner mold increases. The general shape of the $h_o(t)$-curves for these alloys (Fig. 5(b) and 6(b)) are the same as for AC8A and A356 alloys with a wide solidification range.

It is very interesting to note that the temperature measured in the casting near the inner mold (TC3) decreases faster than that near the outer mold (TC4) for the alloys with a congruent melting temperature, while it is reversed, i.e. TC4 decreases faster than TC3 for the alloys with a wide solidification range [Figs. 2(a) and 4(a)]. This is the result of the different behavior of $h_i(t)$ for the two types of alloys. The increasing solidification time with increasing Si-content is attributed to the larger latent heat of solidification of Si.

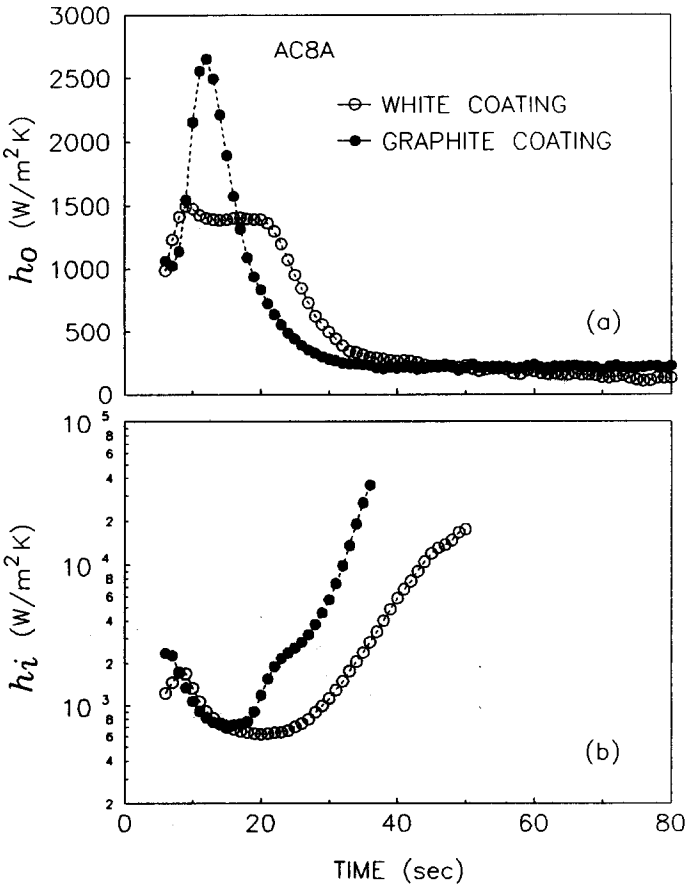

Fig. 3. Comparison of calculated heat transfer coefficients for different coating materials: (a) at the outer and (b) the inner interface.

5. DISCUSSIONS

5.1. *Verification of the calculated heat transfer coefficients*

The verification of the calculated $h_i(t)$ and $h_o(t)$, was accomplished by calculating the temperature in the molds and the casting at various locations and comparing it with the measured temperatures with TC7, 1, 3, 4, 6 and 8. The problem was solved in a straightforward manner using the given initial and the boundary conditions, Equations (3a) and (3b), and Equation (2a) and (2b) with the calculated $h_i(t)$ and $h_o(t)$.

The calculated temperatures of the molds and the casting are shown in Fig. 7, and compared with the corresponding measured ones for the case of AC8A alloy with the graphite coating. A good agreement is obtained between the simulated temperatures and the experimental ones.

5.2. *Summary of the calculated heat transfer coefficients*

The calculated heat transfer coefficients for various casting alloys and coating materials are summarized in Fig. 8. The outside heat transfer coefficient $h_o(t)$ increases rapidly up to a maximum in the initial stage before it decreases due to the gap formation from the moment when a self-sustaining solid (or semi-solid) wall is formed in the outer region of the melt.

The initial increase of $h_o(t)$ can be interpreted in two ways: one is the physically improving contact at the casting/mold interface and the other is the experimental and calculation errors. The major error could probably be the false initial condition of the instantaneous filling and the uniform initial temperatures and a minor error in the delay time in the response of the thermocouple (TC2 and 5 in the present work) used for calculating $h_i(t)$ and $h_o(t)$. The delay time increases as the insulating coating thickness increases, the distance of the thermocouple from the interface increases, and the contact of the thermocouple to the mold becomes worse. A calculation showed that the effect of the delay time in heating the thermocouple under the present experimental condition on the resulting delay in the $h(t)$-increase should be less than 2 s.

On the other hand, the physical contact between the melt and the mold should improve as the melt level increases during pouring and the entrapped air in the interface escapes. However, the major reason for the increase of the interface heat transfer coefficients after pouring is considered partly due to

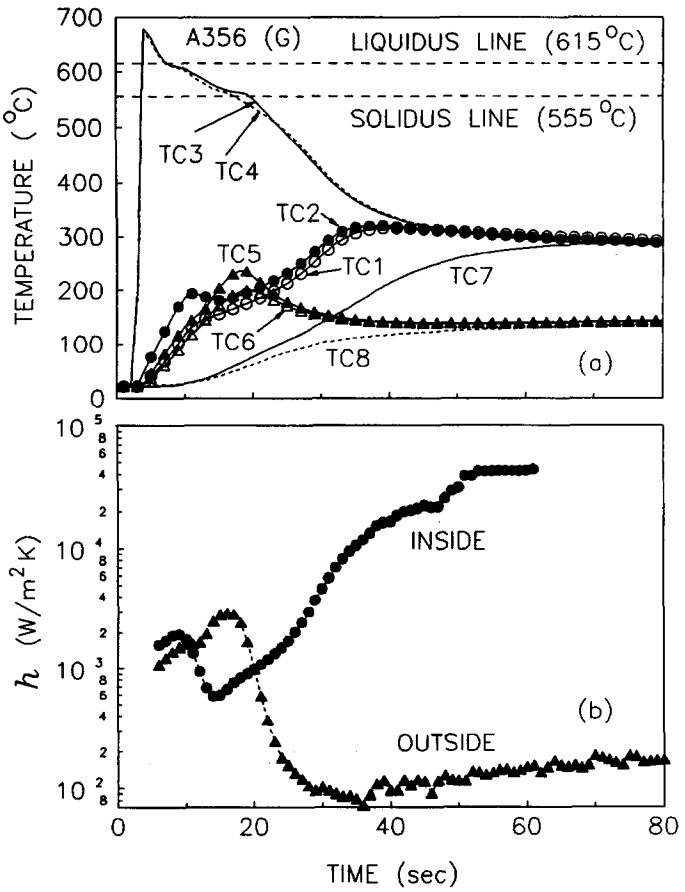

Fig. 4. (a) Measured temperatures vs time for A356 alloy casting; (b) variation of calculated heat transfer coefficients with time.

rapidly increasing thermal conductivity of the air enclosed in the coating and the interface with temperature. For example, the thermal conductivity of the air is 0.026 W m^{-1} K^{-1} at 300 K and increases to 0.052 W m^{-1} K^{-1} at 700 K, a 100% increase. As the surface temperature of the mold increases the temperature and the conductivity of the enclosed air also increase, which increases finally the interface heat transfer coefficients.

The coating is a composite of solid coating materials and air enclosed in voids. The apparent thermal conductivity of the coating can be estimated knowing the thickness of the coating and the maximum heat transfer coefficient, assuming that the maximum value is obtained when there is no gap at the interface. The roughly estimated apparent thermal conductivities of the 70 μm-thick graphite coating and the 100 μm-thick white coating are 0.21 and 0.15 W m^{-1} K^{-1} respectively, which are similar to the data of other works [12, 13]. The graphite coating has a 40% higher thermal conductivity than the white coating. The thermal conductivity of white coating (Foseco Dycote) measured by Jeyarajan and Pehlke [12] increased with increasing thickness from 0.12 W m^{-1} K^{-1} for 25 μm to 0.42 W m^{-1} K^{-1} for 200 μm, which can be explained with the decreasing relative effect of the voids at the surface of the coating as the coating thickness increases.

5.3. *Abnormal behavior of* $h_i(t)$ *for alloys with a wide solidification range*

As shown in Fig. 8(b), the abnormal behavior, i.e. the temporary decrease of $h_i(t)$ is shown only for the alloys with a wide solidification range. The alloys with a wide solidification range solidify generally in a mushy type [8, 14]. Figure 9 shows the typical solidification sequence of the alloys with a congruent melting point [Fig. 9(a)–(c)] and the alloys solidifying in a mushy type [Fig. 9(d)–(f)]. The alloys with a congruent melting point (pure Al and Al–Si binary eutectic) solidify forming a solid shell and the volume shrinkage during the solidification can be easily compensated by the liquid metal between the solid shell, the level of which decreases continuously, and finally a deep shrinkage pipe is formed.

On the other hand, the alloys with the mushy type solidification forms a coherent dendrite network [as shown in Fig. 9(e)] when the solid fraction reaches 10 to 50% depending on the dendrite morphology, which depends again on the composition of the melt and solidification conditions [15, 16]. This coherent dendrite network consists of the bridged dendrites and

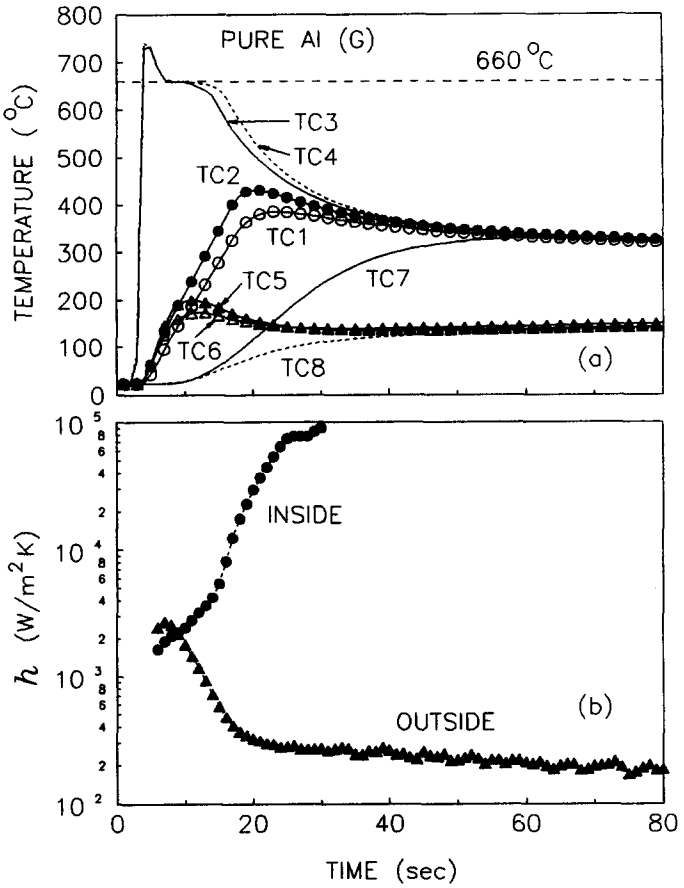

Fig. 5. (a) Measured temperatures vs time for pure Al casting; (b) variation of calculated heat transfer coefficients with time.

once it is formed, the solidification shrinkage can be compensated by the flow of the liquid metal between the dendrites, the so called interdendritic flow [16]. This reveals the skeleton of dendrites slightly on the surfaces of the finished casting, which was confirmed also on the present sample casting of A356 alloy.

As the dendrites become thicker the interdendritic flow requires a larger pressure difference. As can be understood with the aid of Fig. 9(e) the low pressure in the casting, caused by the solidification shrinkage, would pull the coherent dendrite walls on both sides. It is expected that the convex outer wall is stressed compressively and the concave inner wall is exposed to tensional stress. The bridged dendrite network can be pulled apart much easier than being compressed together. Therefore only the inner wall is considered to be pulled outward, i.e. to the inside of the casting and this should create a gap between the inner mold and the casting. The solidification shrinkage of AC8A alloy is about 4% [9] and the compensation of only a small portion of this shrinkage by the collapse of the inner wall is enough to create a gap of for example 50 μm. This kind of shrinkage compensation by the collapse of the coherent dendrite network is called 'burst feeding' [16].

The gap thickness at the inner interface at the moment of the minimum $h_i(t)$ can be calculated by the following equation:

$$h_{tot} = \frac{1}{\frac{1}{h_{gc}+h_{gr}} + \frac{1}{h_c}} \tag{6}$$

where $h_{gc} = k_g/d_g$ is the heat transfer coefficient due to the conduction of the air in the gap, h_{gr} is the heat transfer coefficient due to the radiation across the gap and $h_c = k_c/d_c$ is the heat transfer coefficient due to the conduction of the coating. The h_{gr} is small enough to be neglected compared to the h_{gc} in the present case. The $h_i(t)$ curve for AC8A with the graphite coating in Fig. 8(b) shows a maximum of 2500 W m^{-2} K^{-1} which corresponds to h_c when there is no air gap yet and shows a minimum of 700 W m^{-2} K^{-1} which corresponds to h_{tot} when there is an air gap. Taking the air conductivity at 400°C as 0.05 W m^{-1} K^{-1}, the calculated air gap thickness is about 50 μm. The movement of the inner casting wall of 50 μm corresponds to 0.29% of the total volume, which is a very small fraction of the total solidification shrinkage of 4%. At the moment of the minimum $h_i(t)$ during the experiment, the inner mold could be removed easily by lifting up, which is an evidence of the gap formation by the movement of the inner semi-solid shell.

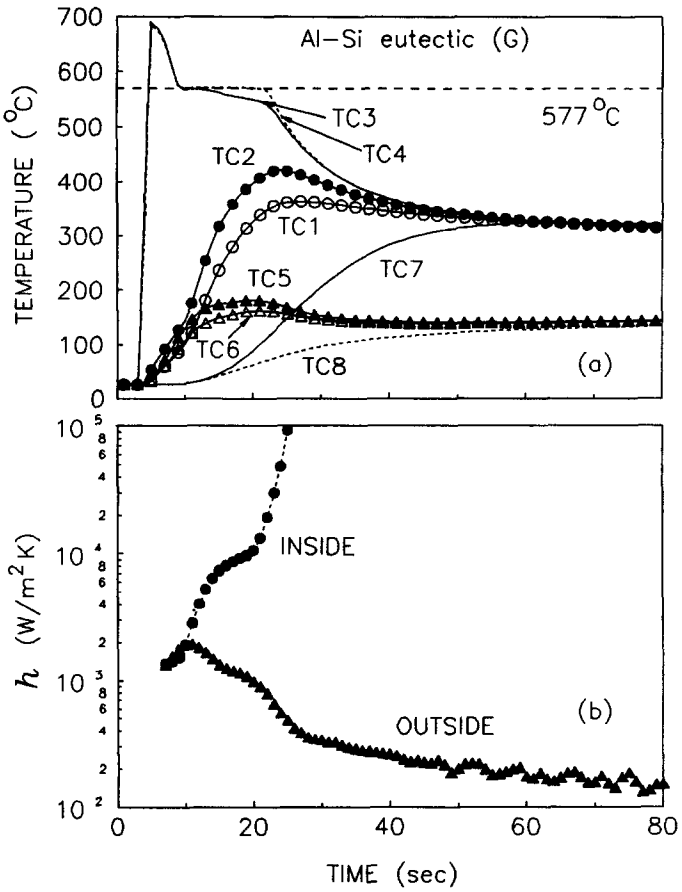

Fig. 6 (a). Measured temperatures vs time for Al–Si binary eutectic alloy casting; (b) variation of calculated heat transfer coefficients with time.

5.4. *Total heat transferred to the molds*

Figure 10 compares the heat flux density and the total heat transferred to the inner and the outer mold for two alloys with different solidification types. Pure Al solidifying with smooth solid shells loses more heat to the inner mold than to the outer mold, while the A356 alloy solidifying in a mushy type loses much less heat to the inner mold, about 50% of that to the outer mold by the end of the solidification time of about 20 s. Yet as the $h_i(t)$ increases very rapidly in the later stage, the heat transferred to the inner mold surpasses finally that to the outer mold. However, the heat transfer until the end of solidification is important for determining the casting structure.

The time-averaged heat transfer coefficients, $\bar{h}_i(t)$ and $\bar{h}_o(t)$, until the end of casting solidification are defined as

$$\bar{h} = \int_0^{t_s} h(t)\,\Delta T\,\mathrm{d}t \Big/ \int_0^{t_s} \Delta T\,\mathrm{d}t, \qquad (7)$$

where $\Delta T = T_{ca} - T_{im}$ (or T_{om}) and t_s is the solidification time at the thermal center of the casting. $\bar{h}_i$ and $\bar{h}_o$ for various casting alloys and coating materials are shown in Table 3. The averaged values presented here can be used for a more simple calculation of the total heat transferred across each interface by the end of solidification.

6. CONCLUSIONS

In order to investigate the characteristics of heat flow for a tube-shaped casting in steel mold and to determine the heat transfer coefficients at the outer and the inner interface, $h_o(t)$ and $h_i(t)$, depending on the alloys, pure Al and three Al base alloys (AC8A, A356 and Al–Si binary eutectic), casting experiments were performed. A computer program was developed on the basis of the inverse heat conduction problem to calculate simultaneously both $h_o(t)$ and $h_i(t)$.

As shown in Fig. 8(a), $h_o(t)$-curves show a similar shape for all alloys, reaching a maximum of around 2900 W m^{-2} K^{-1} for the graphite coating, or 1500 W m^{-2} K^{-1} for the white coating, and then decreasing fast down to around 200 W m^{-2} K^{-1} possibly because of the gap formation at the outer interface due to the thermal expansion of the mold and the thermal contraction of the casting.

The $h_i(t)$-curves, shown in Fig. 8(b), show two distinct behaviours depending on the alloys. The $h_i(t)$ increases continuously for the alloys with congruent

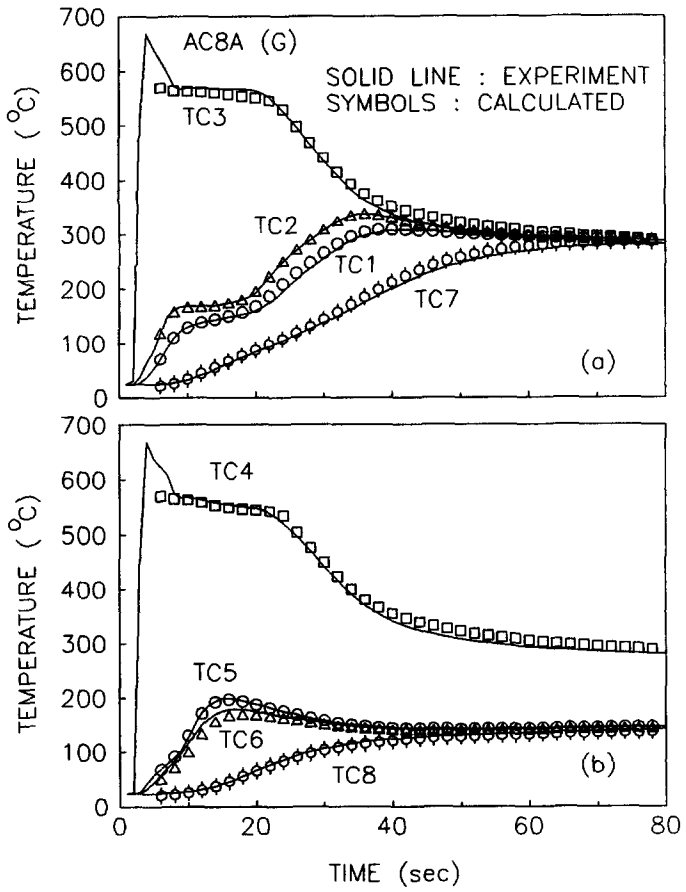

Fig. 7. Comparison of simulated and measured temperatures (a) in the inner mold and the casting; (b) in the outer mold and the casting.

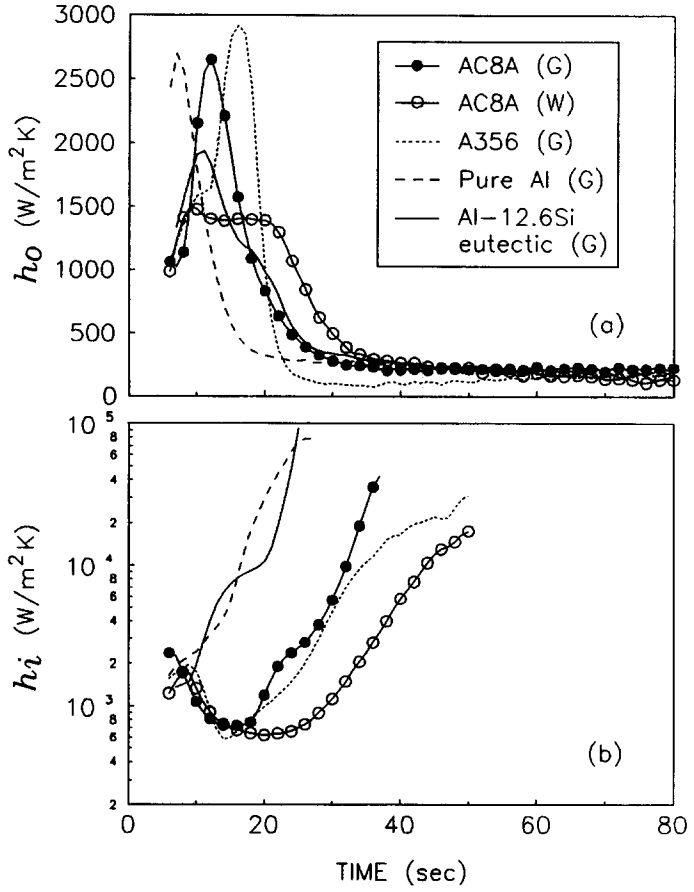

Fig. 8. Summary of the calculated heat transfer coefficients for various casting alloys and coating materials at (a) the outer and (b) the inner interface.

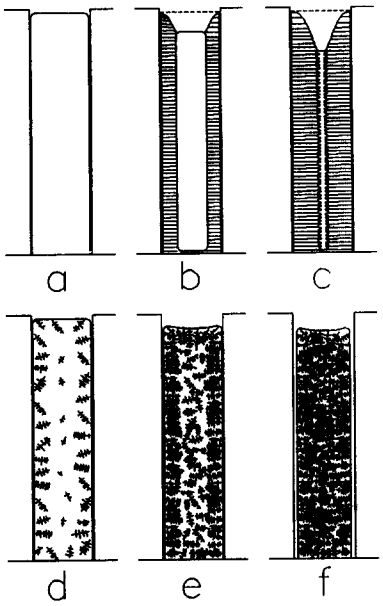

Fig. 9. Solidification sequence of metals with congruent melting point, forming smooth solid shells (a, b, c), and of alloys solidifying in a mushy type (d, e, f), forming coherent dendrite networks.

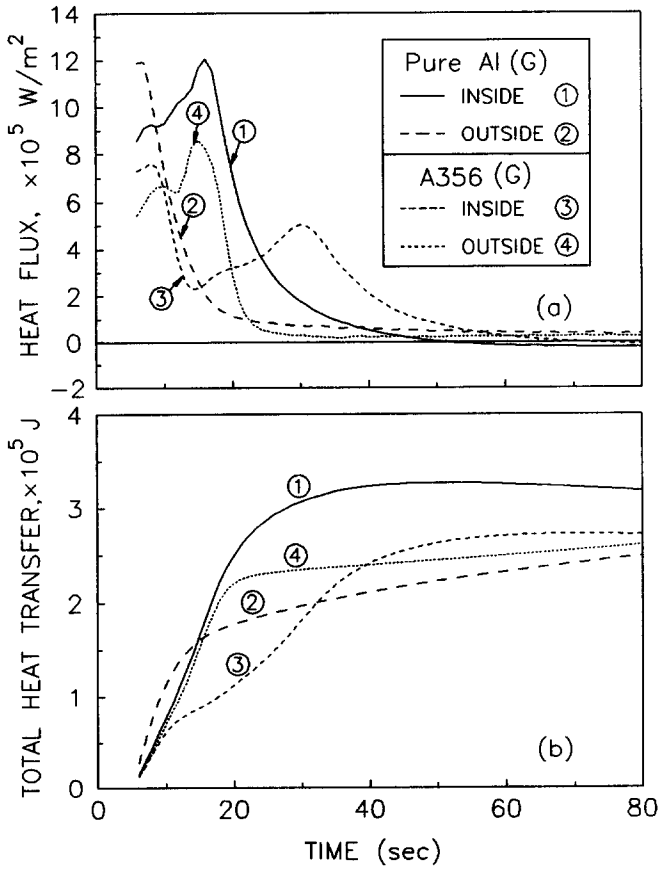

Fig. 10. Comparison of (a) heat flux density, and (b) total heat transferred to the inner and the outer mold for pure Al and A356 alloy.

Table 3. Averaged values of heat transfer coefficients until the end of solidification

	AC8A (G)	AC8A (W)	A356	Pure Al	Al–Si eutectic
$\bar{h}_i$ (W m^{-2} K^{-1})	1180	950	1240	2680	3800
$\bar{h}_o$ (W m^{-2} K^{-1})	1430	1140	1890	1650	1470
Soldification time (t_s, s)	23	32	19	15	20

melting temperature, as expected due to the contraction of the solid shell of the casting on the thermally expanding inner mold. However, the $h_i(t)$ for the alloys with a wide solidification range shows an abnormal behavior, i.e. decreases for a while during the solidification, before it finally increases due to the thermal contraction of the casting. The temporary drop of $h_i(t)$ for the alloys with a wide solidification range should be the result of the solidification contraction, i.e. alloys solidifying in a mushy type form a coherent dendrite network in the early stage of solidification. The low pressure in the casting, created by the solidification contraction, is considered to pull the coherent dendrite wall at the inner side, which creates a gap at the inner interface and decreases $h_i(t)$.

The $h_i(t)$ and $h_o(t)$ data presented here can be used for calculating the transient temperature histories in similar tube-shaped castings of at least similar sizes.

Acknowledgements—The authors greatly appreciate the valuable comments of Professor H. J. Sung, in the department of mechanical engineering at KAIST.

REFERENCES

1. Fletcher, L. S., Recent development in contact conductance heat transfer. *ASME Journal of Heat Transfer*, 1988, **110,** 1059–1070.
2. Nishida, Y., Droste, W. and Engler, S., The air-gap formation process at the casting-mold interface and the heat transfer mechanism through the gap. *Metallurgical Transactions*, 1986, **17B,** 833–844.
3. Stolz, G. Jr., Numerical solutions to an inverse problem of heat conduction for simply shapes. *ASME Journal of Heat Transfer*, 1960, **82,** 20–26.
4. Frank, I., An application of least squares method to the solution of the inverse problem of heat conduction. *ASME Journal of Heat Transfer*, 1963, 378–379.
5. Beck, J. V., Nonlinear estimation applied to the nonlinear inverse heat conduction problem. *International Journal of Heat and Mass Transfer*, 1970, **13,** 703–716.
6. Ho, K. and Pehlke, R. D., Metal-mold interfacial heat transfer. *Metallurgical Transactions*, 1985, **16B,** 585–594.
7. Beck, J. V., Blackwell, B. and St. Clair, C. R., *Inverse Heat Conduction: Ill-posed Problems*. Wiley, New York, 1985.
8. Engler, S., Zur Erstarrungsmorphologie von Aluminium-Gusswerkstoffen. *Aluminum*, 1970, **46,** 121–126.
9. Brandes, E. A., *Smithells Metals Reference Book*, 6th edn. Butterworths, London, 1983.
10. Swaminathan, C. R. and Voller, V. R., Fixed grid techniques for phase change problems: review. *International Journal for Numerical Methods in Engineering*, 1990, **30,** 875–898.
11. Beck, J. V. and Blackwell, B., Inverse problems. In *Handbook of Numerical Heat Transfer*, Chap. 19, ed. W. J. Minkowycz, E. M. Sparrow, G. E. Schneider and R. H. Pletcher. Wiley, New York, 1988.
12. Jeyarajan, A. and Pehlke, R. D., Computer simulation of solidification of a casting with a chill. *Transaction AFS*, 1976, **84,** 647–652.
13. Kumar, T. S. P. and Prabhu, K. N., Heat flux transients at the casting–chill interface during solidification of Al base alloys. *Metallurgical Transactions*, 1991, **22B,** 717–727.
14. Flemings, M. C., *Solidification Processing*. McGraw–Hill, New York, 1974.
15. Chai, G., Bäckerud, L., Rolland, T. and Arnberg, L., Dendrite coherency during equiaxed solidification in binary aluminum alloys. *Metallurgical Transactions*, 1995, **26A,** 965–970.
16. Dahle, A. K. and Arnberg, L., The rheological properties of solidifying Al foundry alloys. *Journal of Metals*, 1996, March, 34–37.